Lidar detection of small aerosol size distribution

Hans D. Hallen, C. Russell Philbrick

Hans D. Hallen, C. Russell Philbrick, "Lidar detection of small aerosol size distribution," Proc. SPIE 10636, Laser Radar Technology and Applications XXIII, 106360J (10 May 2018); doi: 10.1117/12.2304890

SPIE.

Event: SPIE Defense + Security, 2018, Orlando, Florida, United States

Lidar detection of small aerosol size distribution

Hans D. Hallen*, C. Russell Philbrick
Department of Physics, North Carolina State University, Raleigh, NC 27695-8202

ABSTRACT

The major unknown in the global climate radiation balance calculations is the effect of aerosols. The extinction of aerosols depends upon the wavelength, size, concentration, composition, and to a lesser extent, shape of the aerosols. Thus, methods are needed to determine and model these quantities. The size distribution of larger aerosols can be monitored with multistatic lidar, at least in the spherical approximation. We can use this approximation in humid environments, and for old desert dusts in which the aspect ratio is typically below two. Aerosols that are small compared to the incident wavelength present a Rayleigh-like scattering dependence, and the size cannot be determined using multistatic lidar techniques. We discuss the analysis of true extinction from Raman lidar measurements at several wavelengths for determining the size distribution of aerosols. The Angstrom ratio, which is the natural log of the extinction ratio divided by the natural log of the wavelength ratio, has been used in column-integrated measurements to classify aerosols. Lidar backscatter Angstrom ratio measurements have also been used to classify aerosols as a function of range. However, the use for aerosol size distribution has not been investigated in detail before this work. We find, from Raman lidar measurements, Mie models of extinction and backscatter Angstrom ratios, that small aerosols make a significant contribution to optical scattering, and find that size information can be extracted from the lidar data.

Keywords: Lidar, aerosol size distribution, aerosol scattering, extinction, Angstrom ratio, Mie calculations, climate

1. INTRODUCTION

Aerosol properties are important for understanding effects on human health, visibility, and climate forcing [1–7]. Several methods have been developed to measure aerosol properties. Most of these techniques are point-measurements, in which an instrument has to be present in or adjacent to the measurement volume. We discuss here the remote sensing techniques for aerosol particles; in particular, we want to determine their concentration and size distribution [8], although some efforts have been aimed at remote sensing of composition [9]. Remote aerosol active sensing methods are usually optical-based lidar or path integrated signal from a target, and mostly rely on optical extinction measurements. Passive systems use direct or reflected sunlight, or path-integrated extinction between a transmitter and a detector; these techniques often use several wavelengths to obtain information about the aerosol size distribution. Passive satellite measurements (such as MODIS) obtain worldwide coverage, but at the expense of poor time resolution at a location (1-2 days), and relatively coarse vertical resolution near the surface [10–12]. Profiling can only be obtained by analysis at several viewing angles and assumptions about uniformity of the spatial distributions. Active systems can operate either in the path integrated or path profile (lidar) mode, either from orbit (CALIPSO) or from the ground [13–19]. The number of wavelengths used in active systems is usually very small, so less information about the aerosol size distributions can be obtained. We have pursued methods involving bistatic and multistatic lidar [16,20–25] to measure the angular scattering to obtain more information. Using these techniques, we are able to extract distribution properties using parameters from trimodal and lognormal distributions measured remotely. In particular, we found that the ratio of the scattering phase function at the two polarizations can be used to eliminate many of the instrumentation complexities and permit robust measurements [16,20,22–24,26]. The fact that a ratio is used would naively imply that the total scattering, or number of aerosols, would not be obtainable. This is not true, since molecular scattering is also measured, and the known atmospheric molecular density allows a useful quantification of the number of aerosols in the same dataset [27,28]. Multistatic methods fail when the particles are small (in the Raleigh range) compared to the lidar wavelengths. In this case, the scattering angular distribution is that of a dipole, and other methods are needed: the subject of this paper.

We define small aerosols as those for which the angular dependence of scattering is without resonant features, therefore the earlier developments of our multistatic lidar techniques do not apply to them. Figure 1 shows a Mie calculation [8] of several aerosol diameters as a function of angle. It is observed that the size will be very difficult to obtain, without using other factors, for particle diameters below about half of the incident lidar wavelength. Particle diameter/wavelength can provide useful scaling to extrapolate to other lasers from the limit of any observable change at λ=532 nm of d~150 nm.

*hans_hallen@ncsu.edu; phone: 1-919-515-6314; www.physics.ncsu.edu/optics

Laser Radar Technology and Applications XXIII, edited by Monte D. Turner,
Gary W. Kamerman, Proc. of SPIE Vol. 10636, 106360J · © 2018 SPIE
CCC code: 0277-786X/18/$18 · doi: 10.1117/12.2304890

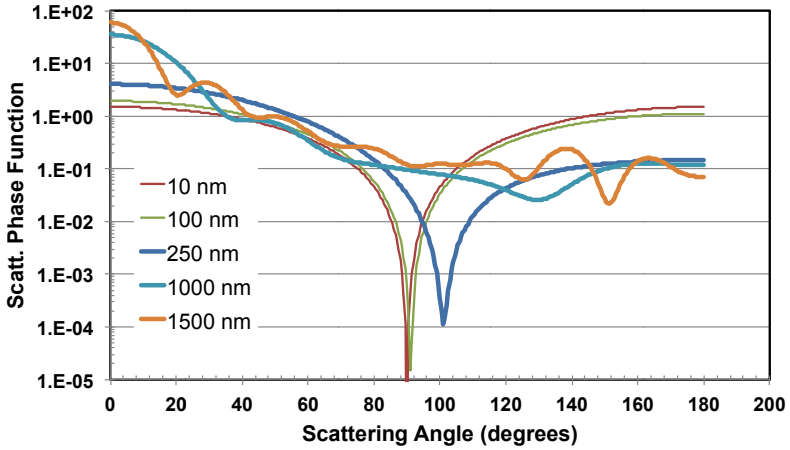

Figure 1. The angle-dependent scattering from water spheres calculated using the Mie formalism indicates the loss of angular scattering resonances (oscillations on the plotted curves) and shows a transition to dipole-like scattering as the particle size decreases. A wavelength of 532 nm is used in this calculation of the particle diameters listed in the legend.

These small particles are very important to characterize, as they are the nucleation mode that can grow to become very important in controlling the radiation balence for climate and physical processes. Their nucleation [29–33], the role of organics [34–36], and subsequent growth [30,37,38] are still active areas of research. Such small particles have scattering cross sections that depend upon the sixth power of the aerosol diameter, see Fig. 2, thus the extinction contribution from the small particles on a per-particle basis is very small. However, there are typically a very large number of such small particles, and we will show that their contribution is appreciable. Typical aerosol distributions [1] include four approximate lognormal contributions: a coarse mode with median diameter >1 micron, an accumulation mode with median diameter ~0.1 to 1.0 microns, the Aitken mode that contains particles typically between 0.01 to 0.1 micron, and the nucleation mode with diameters between clusters of a few molecules to about 10 nm (0.01 μm) diameter. These smaller particle sizes below the accumulation mode are the subject of this paper. Sometimes these small particles are referred to as cloud-condensation nuclei (CCN), when they are large enough that the vapor pressure of water accumulating on them is sufficient to allow further deposition, rather than evaporation. The smallest group of precursor particles, in the nucleation mode, can be as small as a few molecules.

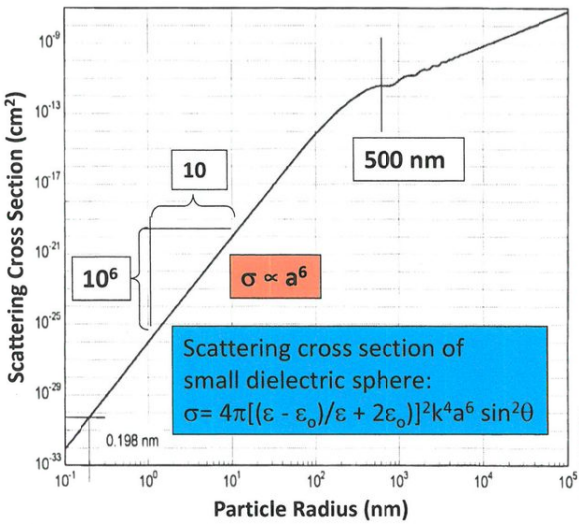

Figure 2. The cross section for scattering by spherical particles is shown as a function of particle radius on a log-log plot. Power laws are linear on such a plot, with slope equal to the exponent. For the 500 nm wavelength of light used in this calculation, the Rayleigh scattering regime begins about half of the wavelength, and is identified as the region with the scattering intensity related to the sixth power of the particle diameter [39].

Clues to how one might proceed to infer distribution properties of the Aitken mode from remote sensing optical measurements can be found by looking at ratios of extinction cross sections, C_{ext} [8], at different wavelengths. Figure 3 indicates that it is important to use real extinction measurements, which can be accurately obtained with a Raman lidar from the gradient of vertical profiles of the primary molecular species (N_2 and O_2 vibrational signatures, or their combination in the rotational signatures), but not with backscatter lidar. The results of Mie calculations of extinction, Fig. 3(a), and backscatter cross section, $C_{backscatter}$, Fig. 3(b), at several pairs of wavelengths for a range of particle diameters are shown. In the Rayleigh regime for both wavelengths, the extinction and backscatter ratios each approach the fourth power of the inverse ratio of the wavelengths used. For example, the 266/532 ratios approach $(532/266)^4 = 16$. The extinction decreases exponentially (linear on the log-linear plot shown) in the regime in which both wavelengths are too long for the Rayleigh range, but the particles are still smaller than about π times the shorter wavelength in diameter. This represents a useful relation to determine diameter from the ratio. The backscatter cross-section ratio has a much narrower range of sensitivity for easily determining size, ending where the Rayleigh regime ends for the shorter wavelength used. We also plot in Fig. 3(b) the cross sections so that the origin of this effect is evident. Although a fit using the response at many wavelengths might allow diameter determination, it will be significantly less robust in the cases of non-mono-sized distributions or deviations from spherical shape than extinction ratios, Fig. 3(a), and therefore we will not consider backscatter further.

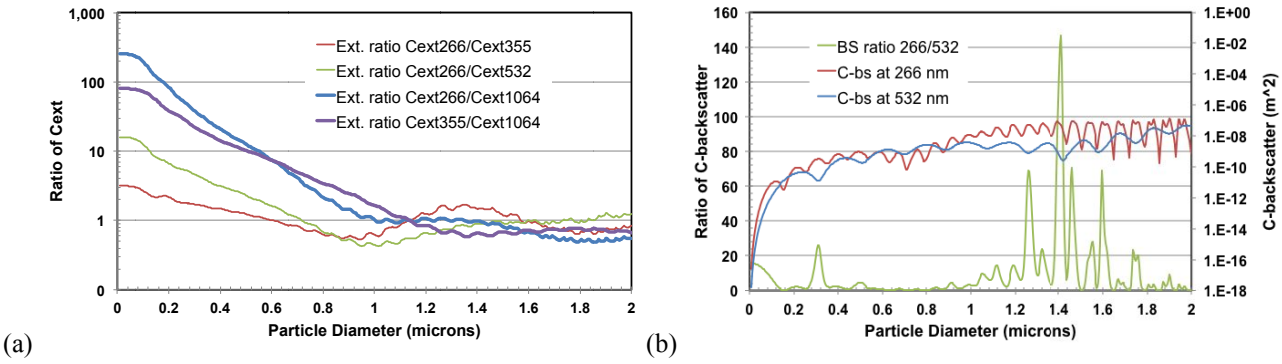

Figure 3. (a) The ratio of extinction from water spheres illuminated by light of different wavelengths is calculated using the Mie formalism. For mono-size-distribution particles for wavelengths roughly between the Rayleigh regime and the particle diameter, the particle size can be determined by the ratio of the extinctions. (b) Backscatter ratio on the same particles is shown for two wavelengths, while the backscatter cross sections, shown on the right axis, are provided for comparison. The region of sensitivity of the proposed technique in (a) exceeds the narrow region from backscatter lidar in (b).

The use of ratios of lidar quantities is not new, as it is related to the Angstrom exponent [40–42] studies, but we will take a different approach to try to obtain particle size distribution information. The Angstrom exponent is given by the logarithm of the ratio of the two quantities at two wavelengths divided by the logarithm of the wavelength ratio. The logarithm makes the Angstrom exponent linear on a linear plot, Fig. 4, while the denominator enforces normalization so that the ratios from different wavelengths are all equal to four for small particles (Rayleigh regime for both wavelengths). Our results are new in that we take the ratio of extinctions and use them for particle sizing. With modern computer analysis techniques, either the simple ratios or their Angstrom coefficients are equally applicable.

It is important to note that to be able to measure the Aitken mode, and especially these precursor aerosols that are most important for our investigation, the shorter of the two wavelengths must be quite small. The particle diameter at which the ratio deviates from its Rayleigh value is determined by the value of the shorter wavelength. This is visible in the plots of Fig. 3(a) and Fig. 4. To obtain information about the important precursor and smaller CCN aerosols, a wavelength near or below the atmospheric transmission window must be selected. Thus, given the limitations of spatial resolution and measurability, ground-based Raman lidar instruments appear to be the only useful approach for these studies.

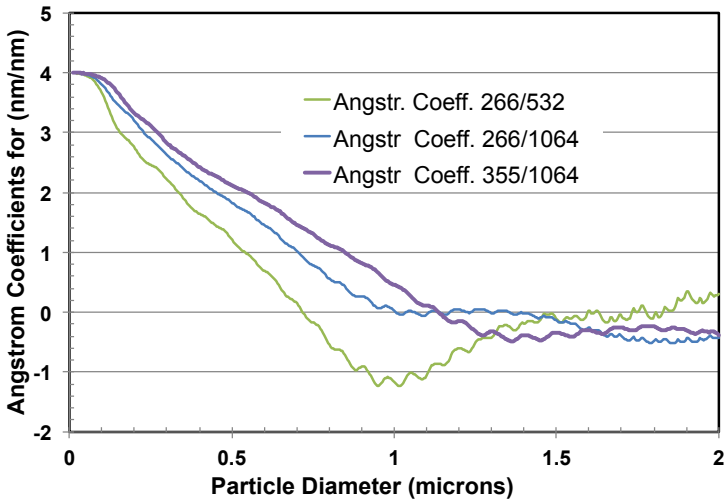

Figure 4. The Angstrom coefficient of extinction from water spheres illuminated by light of different wavelengths is calculated using the Mie formalism. For particles with a size too large for the Rayleigh description to be valid even at the shorter wavelengths used, but smaller than a factor >~1 times the longer wavelength used, the Angstrom coefficient monotonically decreases with particle diameter, thus, that diameter can be determined by this coefficient. Note the similarities between this figure with linear vertical axis and Fig. 3(a) with logarithmic vertical axis.

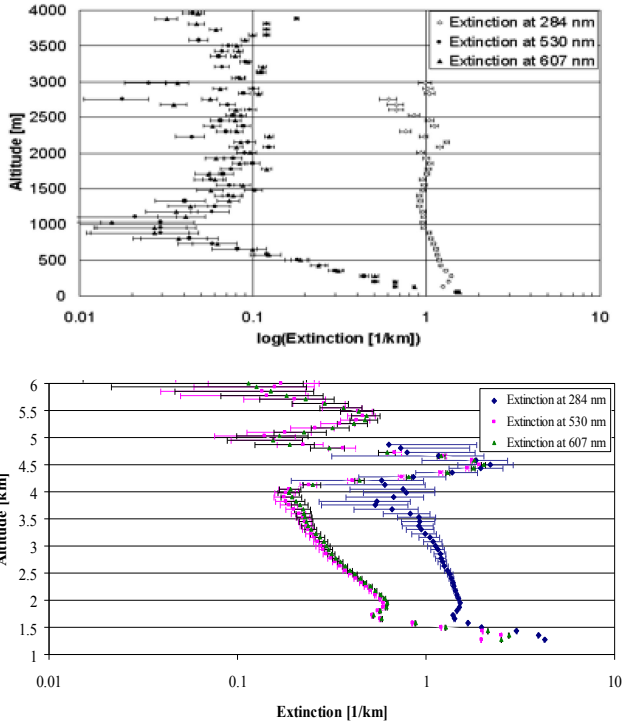

Figure 5. The optical extinction at three wavelengths was measured as a function of altitude with a Raman lidar. (a) Measurements in Philadelphia, PA [43] show Rayleigh-range particles at an altitude above ~1 km. (b) Larger aerosols are found in measurements in Hesperia, CA [15] within a broad altitude range of ~1.5-4 km. The particles are within the range of size sensitivity of the technique. At higher altitudes, multiple scattering in a cloud whitens the scattering and thus extinction, while larger particles are present near the surface.

We next show some measured lidar data that indicates that the small aerosols for which this technique is applicable are, in fact, present and important in the atmosphere. Figure 5 shows Raman lidar data. In Fig. 5(a), extinction vs. altitude data from the NEOPS study near Philadelphia, PA at three different wavelengths shows that, over a wide altitude range above the boundary layer ~1 km, the ratio of the 284 nm extinction to the 530 nm extinction is about a factor of 12, or the frequency ratio to the fourth power. This indicates that very small particles, within the Rayleigh range for both wavelengths, dominate the extinction to 3 km and probably above. At lower altitudes, the ratio drops to a much lower value, in the region of larger boundary layer aerosols. Such behavior is expected, since larger aerosol growth will occur primarily in the boundary layer. Other data from Hesperia, CA, Fig. 5(b), also show small particles aloft, and the extinction ratio from about 1.5 - 4 km altitude is ~10. The results in Fig. 3(a) show that the particle diameters are ~100 nm. The aerosols almost certainly have a broader size distribution, and later we will discuss this effect in the size estimates. To compare to the figure, we make use of the fact that the curves in Fig. 3(a) scale with the wavelength ratio to the fourth power for small aerosols. Thus, we multiply the measurement by a correction factor of $[532/266*284/530]^4 = 1.3$ before comparison. Figure. 5(b) also shows larger aerosols near the surface, and two cloud layers above 4 km

that have a sufficiently high density of larger aerosol particles to cause multiple scattering, which whitens the scattering and hence increases extinction over the full range of wavelengths.

Aerosol spatial distributions can be acquired with a vertical-pointed Raman lidar system, with altitude resolution provided by the lidar ranging and horizontal information from the flow of the atmosphere past the unit. We simultaneously measure water vapor, ozone and temperature in addition to the extinction at several wavelengths. UV extinction measurements have been corrected for the ozone absorption measured in this wavelength range. Figure 6 shows a pair of extinction profiles as a function of time. A comparison reveals a lower layer, 1-2 km in altitude (the site is at 1.2 km elevation) on the right half of the image that exhibits a much stronger extinction at the shorter wavelength, indicating smaller particles present in the sensitivity range of this technique. The ratio of ~3.5 would give a diameter estimate of 0.3 micron from the Fig. 3(a) numbers, corrected for the wavelengths used. Another feature at ~3.4 km in altitude has a higher extinction at the longer wavelength near the center of the images, but about equal extinctions at the very left. This indicates larger particles, larger than the sensitive range of the technique, although multistatic techniques should be able to size them. Between these two layers, the ratio is large, suggesting small particles.

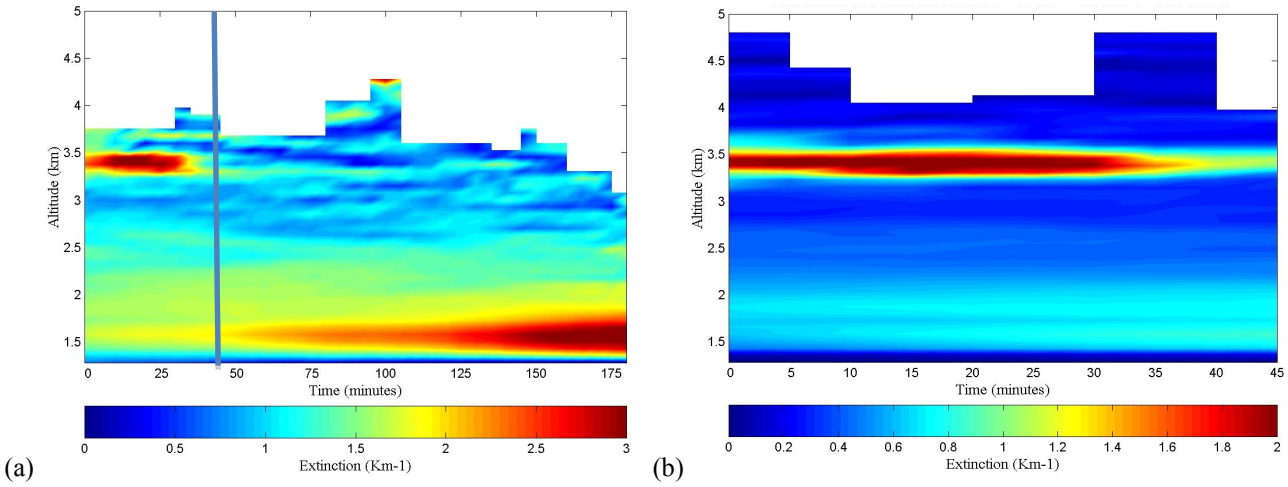

Figure 6. Extinction vs. time and altitude in Hesperia, CA is measured by a vertical Raman lidar system. (a) 284 nm, (b) 530 nm [44]. The vertical line in (a) marks the beginning of daylight and end of the part (b) data.

Figure 7 shows measurements on the next night (these data start about midnight local time), the situation was a little different. There is no cloud precursor at higher altitudes, and the aerosols at ~1.5 km are a little larger. There still is a region of a high concentration of small aerosols up to 3.5 km, particularly during the first two hours of the measurement.

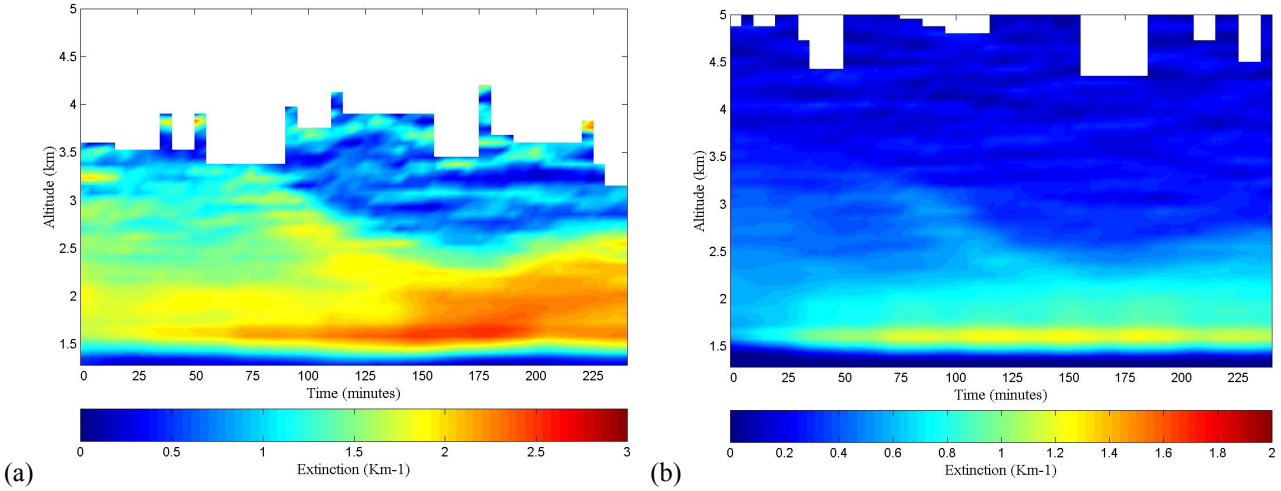

Figure 7. Extinction vs. time and altitude in Hesperia, CA is measured by a vertical Raman lidar system. (a) 284 nm, (b) 530 nm. [44]

Real aerosols in the atmosphere are not mono-dispersed, but are found in distributions often modeled as lognormal distributions as discussed above. We consider a single lognormal distribution of small aerosols and investigate the impact of the distribution on the applicability of a simple technique such as indicated in Fig. 3(a). To begin, we follow a procedure similar to that used for Fig. 3, but rather than change the size of a single particle, we change the median of a distribution. The lognormal distribution parameters we choose are similar to those we have measured for small aerosols before. These parameters and results will be shown after we review the lognormal distribution itself.

The normalized lognormal distribution is characterized by two parameters, the position parameter, μ, and the width parameter, σ. We use a slightly different definition of the position parameter than the most common definition since we do not like having units in the logarithm function, and both the position parameter and the size axis have units of length, which need to cancel inside. We thus use a scaling factor, N, for the number of aerosols per volume,

$$lognorm(x) = \frac{N}{x\sigma\sqrt{2\pi}} exp\left(-0.5\left(\frac{ln\left(\frac{x}{\mu}\right)}{\sigma}\right)^2\right). \quad (1)$$

This has mean $\mu exp\,(0.5\sigma^2)$, mode $\mu exp\,(-\sigma^2)$, and median μ. In the study that follows, we vary the median (position parameter) and fix the width parameter at 0.4. The number density cancels in the ratios, so its value is moot. Figure 8(a) shows the two lognormal distributions (normalized for one particle) at the ends of the range used in Fig. 8(b). The latter figure is the equivalent, with a size distribution rather than a single particle size, to Fig 3(a). The general tendencies are the same, but the value at the lower end of the size range is smaller, and the functions drop to ~1 (the end of the range of sensitivity) at smaller sizes. These effects are expected, since the distribution represents a weighted average of the data in Fig. 3(a). Since the curves decrease, averaging reduces the values on the left. Further, the width of the distribution implies that larger particles are present. The sensitivity is expected to be lost when a sufficient weight of the larger particles is beyond the wavelength, or out of range in Fig. 3(a). As the median increases, so does the width for fixed width parameter, so many particles are larger than the median. On the small particle end, nucleation mode distributions such as the first one used, Fig. 8(a), are in the sensitive region, Fig. 8(b).

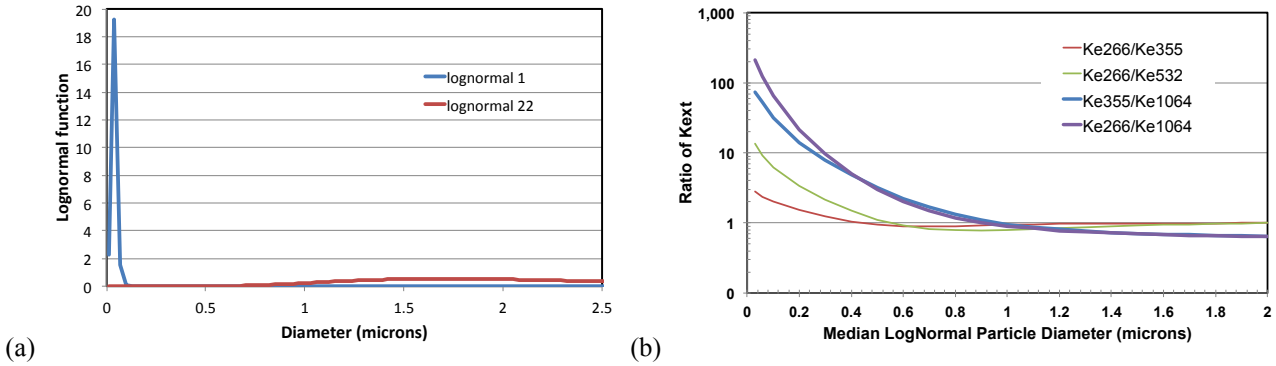

(a) (b)

Figure 8. The impact of a lognormal aerosol distribution (here) instead of mono-dispersed aerosols (Fig. 3(a)) is considered; (a) the smallest and largest median lognormal distributions used. They are normalized to one particle each and both have the same 0.4 width parameter, while the medians are 0.03 and 2.0. (b) The qualitative aspects of the mono-size distribution are retained, although the scaling and sensitive size regime is reduced. The extinction parameter k_{ext} is the weighted average of C_{ext}*(Number Density) over the size distribution, not including any molecular contribution.

The obvious question to ask is whether the distribution properties can be extracted from these ratios. There are two parameters that should be extractable from the ratios in the absence of molecular contribution. Likely, all three, including number density, can be identified in the presence of the molecular scattering, as was possible in the multi-static case discussed above. We need an equal or greater number of observations than parameters to extract, so the ratio at several wavelength pairs will be required -- essentially we will need extinction measurements at 3-4 wavelengths that are far enough apart to give independent values. A complete study of this is beyond the scope of this paper and will be addressed in future work.

To further motivate the applicability for using this approach to determine the size distributions, we now discuss a study for which extinction was measured at several wavelengths through a test chamber that had controlled injection of desert dust with simultaneous aerosol size distribution measurement. The extinction measurements used in the Fig. 9 calculations were described before [45]. We can analyze these data from two directions: (1) the extinction measurements can be used to directly extract the ratios of the extinction coefficients k_{ext}, and (2) the size distributions can be input into Mie calculations with measured indices of refraction for the particles [46]. The determination of measured indices avoided scattering and index of refraction variation artifacts (see reference [46]). The same quantities are obtained from each approach, and we can evaluate consistency. The consistency we find supports the idea of future efforts to determine the distributions from extinction measurements at several wavelengths, which will be especially useful for small particles in the nucleation mode whose distributions cannot be determined with established remote sensing methods.

The extinction measurements are acquired before, during, and after injecting dust to create the aerosols. As soon as the dust is in the air, the larger particles will start to settle, so we seek to find the values shortly after injection when they are closest to lognormal functions, which is what we model. The k_{ext} is determined from the logarithm of the signal decrease due to the dust, scaled by the chamber length and units conversions. Plots of the extinction coefficient values for 100 seconds after injection of dust are shown in Fig. 9 for three wavelengths. The steady value after the rise (injection) is taken as the k_{ext} for comparison. Note the change afterwards, likely due to the loss of larger particles.

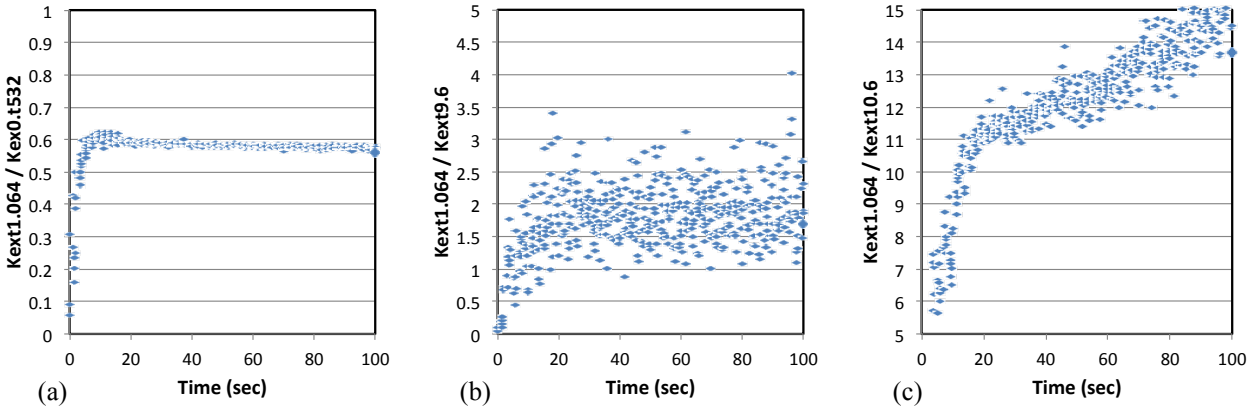

Figure 9. The extracted extinction coefficient ratios relative to that of 1.064 micron wavelength: (a) 532 nm wavelength gives 0.6, (b) 9.6 microns gives ~2, and (c) 10.6 microns gives ~11.

The measured distributions were least-squares fit to a single lognormal distribution. Median values were close to 1.16 microns and width parameters near 0.4. The number varied, but will cancel in the ratio calculation. The biggest discrepancy in the fit occurred above 2 microns; where the measured values always fell below the lognormal prediction, presumably due to settling. To compensate for this, we did not model particles larger than 2.5 microns in diameter. These distributions of nominal 0-3 micron diameter dust, contained particles large enough that calculations involving 266, 355, and 532 nm wavelengths all had ratios near 1, so out of the range of sensitivity, Figs. 8(b) and 9(a). We thus used ratios against 1.024 microns, and the other measured wavelengths of 9.6 and 10.6 microns. The predicted ratios using the distributions and n+ik of 1.45+0.003i, 1.75+0.9i, and 1.67+0.25i for 1.064, 9.6, and 10.6 micron wavelengths, respectively, gave ratios k_{ext} 9.6/k_{ext} 1.064 = 3.7 (2 from Fig. 9) and k_{ext} 10.6/k_{ext} 1.064 = 13.1 (11 from Fig. 9). The agreement is reasonable, suggesting the robustness of the method.

In summary, we present an approach to determine the size of small aerosols via Raman-lidar-measured extinction ratios at several wavelengths. Mie modeling, and the presence and importance of such small aerosols identified with existing Raman lidar data, supported the choice of this measurement technique and analysis method. The effects of particle distributions were considered using Mie calculations and closure obtained from measurements of extinction at several wavelengths in conjunction with aerosol size distributions. One of the exciting results is the expectation that this approach can be extended to the nucleation mode size distribution.

REFERENCES

[1] Colbeck, I. and Lazaridis, M., "Aerosols and environmental pollution," Naturwissenschaften **97**(2), 117–131 (2010).

[2] Levin, Z. and Cotton, W. R., eds., [Aerosol pollution impact on precipitation: a scientific review], Springer, Dordrecht ; London (2009).

[3] Fan, J., Rosenfeld, D., Zhang, Y., Giangrande, S. E., Li, Z., Machado, L. A. T., Martin, S. T., Yang, Y., Wang, J., Artaxo, P., Barbosa, H. M. J., Braga, R. C., Comstock, J. M., Feng, Z., Gao, W., Gomes, H. B., Mei, F., Pöhlker, C., Pöhlker, M. L., et al., "Substantial convection and precipitation enhancements by ultrafine aerosol particles," Science **359**(6374), 411–418 (2018).

[4] Philbrick, C. R. and Hallen, H., "Measurements of contributors to atmospheric climate change," Proceedings of the 19th ESA Symposium on European Rocket and Balloon Programmes and Related Research, 141–146, Noordwijk, Netherlands (2009).

[5] Colbeck, I. and Lazaridis, M., eds., [Aerosol science: technology and applications], Wiley, Chichester, West Sussex, United Kingdom (2014).

[6] Andreae, M. O. and Rosenfeld, D., "Aerosol–cloud–precipitation interactions. Part 1. The nature and sources of cloud-active aerosols," Earth-Science Reviews **89**(1–2), 13–41 (2008).

[7] Seinfeld, J. H. and Pandis, S. N., [Atmospheric chemistry and physics: from air pollution to climate change, Third edition], John Wiley & Sons, Inc, Hoboken, New Jersey (2016).

[8] Bohren, C. F. and Huffman, D. R., [Absorption and scattering of light by small particles], Wiley-VCH, Weinheim (2004).

[9] Niu, S., Philbrick, C. R. and Hallen, H. D., "Remote aerosol species-identification using IR scattering spectroscopy," Proceedings of the SPIE - The International Society for Optical Engineering **9080**, 908010 (12 pp.), USA (2014).

[10] Lacagnina, C., Hasekamp, O. P. and Torres, O., "Direct radiative effect of aerosols based on PARASOL and OMI satellite observations: DREA based on PARASOL/OMI," Journal of Geophysical Research: Atmospheres **122**(4), 2366–2388 (2017).

[11] Dubovik, O., Holben, B., Eck, T. F., Smirnov, A., Kaufman, Y. J., King, M. D., Tanré, D. and Slutsker, I., "Variability of Absorption and Optical Properties of Key Aerosol Types Observed in Worldwide Locations," J. Atmos. Sci. **59**(3), 590–608 (2002).

[12] Russell, P. B., Kacenelenbogen, M., Livingston, J. M., Hasekamp, O. P., Burton, S. P., Schuster, G. L., Johnson, M. S., Knobelspiesse, K. D., Redemann, J., Ramachandran, S. and Holben, B., "A multiparameter aerosol classification method and its application to retrievals from spaceborne polarimetry," J. Geophys. Res. Atmos. **119**(16), 2013JD021411 (2014).

[13] Burton, S. P., Ferrare, R. A., Hostetler, C. A., Hair, J. W., Rogers, R. R., Obland, M. D., Butler, C. F., Cook, A. L., Harper, D. B. and Froyd, K. D., "Aerosol classification using airborne High Spectral Resolution Lidar measurements – methodology and examples," Atmos. Meas. Tech. **5**(1), 73–98 (2012).

[14] Dreischuh, T., Grigorov, I., Peshev, Z., Deleva, A., Kolarov, G. and Stoyanov, D., "Lidar Mapping of Near-Surface Aerosol Fields," [Aerosols - Science and Case Studies], K. Volkov, Ed., InTech (2016).

[15] Verghese, S. J., Willitsford, A. H. and Philbrick, C. R., "Raman lidar measurements of aerosol distribution and cloud properties," Lidar Remote Sensing for Environmental Monitoring VI, Vol. 5887, SPIE Proceedings, 58870H 1-8 (2005).

[16] Philbrick, C. R., Wyant, A. M., Verghese, S., Edwards, P. S., and Wright, T., "Characteristics of Atmospheric Aerosols Based on Optical Remote Sensing," 90th AMS, 12th Conf. Atmos. Chem., 1–8, Atlanta, GA (2010).

[17] Itahashi Syuichi, Yumimoto Keiya, Uno Itsushi, Eguchi Kenta, Takemura Toshihiko, Hara Yukari, Shimizu Atsushi, Sugimoto Nobuo and Liu Zhaoyan., "Structure of dust and air pollutant outflow over East Asia in the spring," Geophysical Research Letters **37**(20) (2010).

[18] von Zahn, U., von Cossart, G., Fiedler, J., Fricke, K. H., Nelke, G., Baumgarten, G., Rees, D., Hauchecorne, A. and Adolfsen, K., "The ALOMAR Rayleigh/Mie/Raman lidar: objectives, configuration, and performance," Ann. Geophys. **18**(7), 815–833 (2000).

[19] McKeever, K. R., Greenert, K. L. and Philbrick, C. R., "Characterization of noctilucent clouds utilizing a ten-channel photometer," 18th ESA Symposium on European Rocket and Balloon Programmes and Related Research, 133–138, Noordwijk, Netherlands (2007).

[20] Stevens, T. D. and Philbrick, C. R., "Atmospheric extinction from Raman lidar and a bi-static remote receiver," Second Topical Symposium on Combined Optical-Microwave Earth and Atmosphere Sensing, IEEE Proceedings, 170–173, IEEE (1995).
[21] Stevens, T. D. and Philbrick, C. R., "Particle size distributions and extinction determined by a unique bistatic lidar technique," Geoscience and Remote Sensing Symposium, IGARSS '96. "Remote Sensing for a Sustainable Future." **2**, 1253–1256, IEEE (1996).
[22] Novitsky, E. J., "Multistatic lidar profiling of urban atmospheric aerosols," Journal of Geophysical Research **110**, D7511, 1-11 (2005).
[23] Wyant, A. M., Brown, D. M., Edwards, P. S. and Philbrick, C. R., "Multi-wavelength multi-angular lidar for aerosol characterization," Laser Radar Technology and Applications XIV, Vol. 7323, SPIE Proceedings, M. D. Turner and G. W. Kamerman, Eds., 73230R 1-8 (2009).
[24] Brown, A. M., Snyder, M. G., Brouwer, L. and Philbrick, C. R., "Atmospheric aerosol characterization using multiwavelength multistatic light scattering," Laser Radar Technology and Applications XV, Vol. 7684, SPIE, 76840I 1-11 (2010).
[25] Hallen, H. D., Long, B. J. N., Hook, D. A., Pangle, G. E. and Philbrick, C. R., "Multistatic lidar measurements of non-spherical aerosols," Proceedings SPIE Laser Radar Technology and Applications XVIII, Vol. 8731, 87310P, Baltimore, MD (2013).
[26] Long, B. J. N., Hook, D. A., Pangle, G. E., Hallen, H. D. and Philbrick, C. R., "Using a laser aureole to study aerosols," Proceedings SPIE Laser Radar Technology and Applications XVIII, Vol. 8731, 87310O, Baltimore, MD (2013).
[27] Snyder, Michelle., "Characterization of Aerosols Using Multiwavelength Multistatic Optical Scattering Data," North Carolina State University, Doctor of Philosophy (2011), http://www.lib.ncsu.edu/resolver/1840.16/7010.
[28] Snyder, M. G., Brown, A. M. and Philbrick, C. R., "Sensitivity of the polarization ratio method to aerosol concentration," Laser Radar Technology and Applications XVI, Vol. 8037, SPIE, 80370K 1-15 (2011).
[29] McMurry, P. H. and Friedlander, S. K., "New particle formation in the presence of an aerosol," Atmospheric Environment (1967) **13**(12), 1635–1651 (1979).
[30] Hodshire, A. L., Lawler, M. J., Zhao, J., Ortega, J., Jen, C., Yli-Juuti, T., Brewer, J. F., Kodros, J. K., Barsanti, K. C., Hanson, D. R., McMurry, P. H., Smith, J. N. and Pierce, J. R., "Multiple new-particle growth pathways observed at the US DOE Southern Great Plains field site," Atmos. Chem. Phys. **16**(14), 9321–9348 (2016).
[31] Hoppel W. A., Frick G. M., Fitzgerald J. W. and Larson R. E., "Marine boundary layer measurements of new particle formation and the effects nonprecipitating clouds have on aerosol size distribution," Journal of Geophysical Research: Atmospheres **99**(D7), 14443–14459 (2012).
[32] Weber, R. J., Marti, J. J., McMurry, P. H., Eisele, F. L., Tanner, D. J. and Jefferson, A., "Measured atmospheric new particle formation rates: implications for nucleation mechanisms," Chemical Engineering Communications **151**(1), 53–64 (1996).
[33] Yu, H., Ortega, J., Smith, J. N., Guenther, A. B., Kanawade, V. P., You, Y., Liu, Y., Hosman, K., Karl, T., Seco, R., Geron, C., Pallardy, S. G., Gu, L., Mikkilä, J. and Lee, S.-H., "New Particle Formation and Growth in an Isoprene-Dominated Ozark Forest: From Sub-5 nm to CCN-Active Sizes," Aerosol Science and Technology **48**(12), 1285–1298 (2014).
[34] Metzger, A., Verheggen, B., Dommen, J., Duplissy, J., Prevot, A. S. H., Weingartner, E., Riipinen, I., Kulmala, M., Spracklen, D. V., Carslaw, K. S. and Baltensperger, U., "Evidence for the role of organics in aerosol particle formation under atmospheric conditions," PNAS (2010).
[35] Zhang, R., Suh, I., Zhao, J., Zhang, D., Fortner, E. C., Tie, X., Molina, L. T. and Molina, M. J., "Atmospheric New Particle Formation Enhanced by Organic Acids," Science **304**(5676), 1487–1490 (2004).
[36] Weber, R. J., Marti, J. J., McMurry, P. H., Eisele, F. L., Tanner, D. J. and Jefferson, A., "Measurements of new particle formation and ultrafine particle growth rates at a clean continental site," Journal of Geophysical Research: Atmospheres **102**(D4), 4375–4385 (1997).
[37] Kaiser, J. C., Hendricks, J., Righi, M., Riemer, N., Zaveri, R. A., Metzger, S. and Aquila, V., "The MESSy aerosol submodel MADE3 (v2.0b): description and a box model test," Geoscientific Model Development **7**(3), 1137–1157 (2014).
[38] McMurry, P. H. and Friedlander, S. K., "Aerosol formation in reacting gases: Relation of surface area to rate of gas-to-particle conversion," Journal of Colloid and Interface Science **64**(2), 248–257 (1978).
[39] Li, Guangkun., "Atmospheric Aerosol and Particle Properties Using Lidar," The Pennsylvania State University, Doctor of Philosophy (2003), http://www.crphilbrick.org/showpaper.php?showpaperid=99.

[40] Kaskaoutis, D. G., Kambezidis, H. D., Hatzianastassiou, N., Kosmopoulos, P. G. and Badarinath, K. V. S., "Aerosol climatology: dependence of the Angstrom exponent on wavelength over four AERONET sites," Atmos. Chem. Phys. Discuss. **2007**, 7347–7397 (2007).
[41] Russell, P. B., Bergstrom, R. W., Shinozuka, Y., Clarke, A. D., DeCarlo, P. F., Jimenez, J. L., Livingston, J. M., Redemann, J., Dubovik, O. and Strawa, A., "Absorption Angstrom Exponent in AERONET and related data as an indicator of aerosol composition," Atmos. Chem. Phys. **10**(3), 1155–1169 (2010).
[42] Schuster, G. L., Dubovik, O. and Holben, B. N., "Angstrom exponent and bimodal aerosol size distributions," Journal of Geophysical Research **111**(D7) (2006).
[43] Philbrick, C. R. and Mulik, K. R., "Application of Raman lidar to air quality measurements," Laser Radar Technology and Applications V, Vol. Vol. 4035, SPIE, pp. 22-33 (2000).
[44] Sachin John Verghese., "Investigation of aerosol and cloud properties using multiwavelength raman lidar measurements," The Pennsylvania State University, Ph.D. Dissertation (2008), https://etda.libraries.psu.edu/catalog/8382.
[45] Pangle, G. E., Hook, D. A., Long, B. J. N., Philbrick, C. R. and Hallen, H. D., "Optical extinction dependence on wavelength and size distribution of airborne dust," Proceedings SPIE Laser Radar Technology and Applications XVIII, Baltimore, MD, Vol. 8731, 87310N, pp. 1-14, (2013).
[46] Hook, D. A., Pangle, G. E., Long, B. J. N., Philbrick, C. R. and Hallen, H. D., "Understanding lidar returns from complex dust mixtures," Proceedings SPIE Laser Radar Technology and Applications XVIII, Baltimore, MD, Vol. 8731, 87310M pp. 1-12 (2013).